Phenylalanine 393 Exerts Thermodynamic Control over the Heme of Flavocytochrome P450 BM3[†]

Tobias W. B. Ost,*[,‡] Caroline S. Miles,[§] Andrew W. Munro,[||] Jane Murdoch,[§] Graeme A. Reid,[§] and Stephen K. Chapman[‡]

Department of Chemistry, University of Edinburgh, West Mains Road, Edinburgh, EH9 3JJ, U.K., Institute of Cell and Molecular Biology, University of Edinburgh, Mayfield Road, Edinburgh, EH9 3JT, U.K., and Department of Biochemistry, The Adrian Building, University of Leicester, University Road, Leicester, LE1 7RH, U.K.

Received April 9, 2001; Revised Manuscript Received September 4, 2001

ABSTRACT: Site-directed mutants of the phylogenetically conserved phenylalanine residue F393 were constructed in flavocytochrome P450 BM3 from *Bacillus megaterium*. The high degree of conservation of this residue in the P450 superfamily and its proximity to the heme (and its ligand Cys400) infers an essential role in P450 activity. Extensive kinetic and thermodynamic characterization of mutant enzymes F393A, F393H, and F393Y highlighted significant differences from wild-type P450 BM3. All enzymes expressed to high levels and contained their full complement of heme. While the reduction and subsequent treatment of the mutant P450s with carbon monoxide led to the formation of the characteristic P450 spectra in all cases, the absolute position of the Soret absorption varied across the series WT/F393Y (449 nm), F393H (445 nm), and F393A (444 nm). Steady-state turnover rates with both laurate and arachidonate showed the trend WT > F393Y ≫ F393H > F393A. Conversely, the trend in the pre-steady-state flavin-to-heme electron transfer was the reverse of the steady-state scenario, with rates varying F393A > F393H ≫ F393Y ≈ wild-type. These data are consistent with the more positive substrate-free [−312 mV (F393A), −332 mV (F393H)] and substrate-bound [−151 mV (F393A), −176 mV (F393H)] reduction potentials of F393A and F393H heme domains, favoring the stabilization of the ferrous-form in the mutant P450s relative to wild-type. Elevation of the heme iron reduction potential in the F393A and F393H mutants facilitates faster electron transfer to the heme. This results in a decrease in the driving force for oxygen reduction by the ferrous heme iron, so explaining lower overall turnover of the mutant P450s. We postulate that the nature of the residue at position 393 is important in controlling the delicate equilibrium observed in P450s, whereby a tradeoff is established between the rate of heme reduction and the rate at which the ferrous heme can bind and, subsequently, reduce molecular oxygen.

The cytochromes P450[1] are a superfamily of heme *b*-containing monooxygenase enzymes (*1*). They are widespread in all life forms (from bacteria through to man) and are notable for their diversity in substrate selectivity. The best understood P450 systems are the bacterial P450cam (camphor hydroxylase from *Pseudomonas putida*) and P450 BM3 (fatty acid hydroxylase from *Bacillus megaterium*) (*2*, *3*). Study of the crystal structures (*4*, *5*) of these soluble enzymes has enabled the design of site-directed mutants, allowing the roles of several key amino acids to be determined. Despite similar tertiary structure, these two enzymes belong to two different classes of P450. P450cam is a class I (or B-class) P450, receiving electrons from a two component reductase system (ferredoxin and NADH-ferredoxin reductase) (*6*). P450 BM3 is a class II (or E-class) P450, receiving electrons from a eukaryotic-like diflavin NADPH-cytochrome P450 reductase fused to the P450 in one continuous polypeptide (*7*). This fused arrangement of its redox partners correlates with the high catalytic activity of P450 BM3 and makes the system very convenient as a model for mechanistic studies of P450s and P450-related enzymes (such as the nitric oxide synthases) (*8*).

Comparisons of the amino acid sequences of all P450s reveal only a few residues which are implicitly conserved throughout the superfamily. One of these is the cysteine that provides the thiolate ligand to the heme iron (Cys400 in P450 BM3) (Figure 1). In addition there are several residues, located close to this ligand, which display high conservation within what is termed the "heme binding" motif (9). A phenylalanine residue (F393 in P450 BM3) is almost totally conserved within this region, with a small number of exceptions, including the dehydratase P450 74 (an allene oxide synthase from flax seed) and P450 10 from the pond snail *Lymnaea stagnalis*, with potential involvement in steroid synthesis (*10*, *11*). The analogous residues are proline and tryptophan, respectively. This high level of conservation

[†] The research was performed with support from the Edinburgh Protein Interaction Centre (EPIC), the BBRSC (studentship to T.W.B.O. and Postdoctoral funding to C.S.M. and J.M.), The Royal Society of Edinburgh and the Leverhulme Trust (A.W.M.).

* To whom correspondence should be addressed. Phone: +44 131 6507386. Fax: +44 131 6504760. E-mail: skc03@holyrood.ed.ac.uk.

[‡] Department of Chemistry.

[§] Institute of Cell and Molecular Biology.

[||] Department of Biochemistry.

[1] Abbreviations: P450, cytochrome P450 monooxygenase; PMSF, phenylmethanesulfonyl fluoride; SHE, standard hydrogen electrode; Δ*G*, Gibbs' free-energy NOS, nitric oxide synthase.

10.1021/bi010716m CCC: $20.00
Published on Web 10/20/2001

Cyp101 (cam)	345	V	S	H	T	T	F	G	H	G	S	H	L	C	L	G	Q	H	L	362
Cyp102 (BM3)	388	H	A	F	K	P	F	G	N	G	Q	R	A	C	I	G	Q	Q	F	405
Cyp6A1 (Housefly)	437	L	D	W	L	G	F	G	D	G	P	R	N	C	I	G	M	R	F	444
Cyp2E1 (Rabbit)	425	D	Y	F	K	P	F	S	A	G	K	R	V	C	V	G	E	G	L	442
Cyp11A1 (Human)	450	F	R	N	L	G	F	G	W	G	V	R	Q	C	L	G	R	R	I	467
Cyp74 (flaxseed)	477	P	E	T	E	T	P	S	V	A	N	K	Q	C	A	G	K	D	F	494
Cyp10 (snail)	481	T	S	Q	L	V	W	G	H	G	A	R	M	C	L	G	R	R	I	499

FIGURE 1: Sequence alignment within the heme-binding region of selected P450s (*2*, *26*−*29*). The alignment shows the implicitly conserved cysteine residue which provides the sixth ligand to the heme iron of all P450s (dotted box). Seven residues downstream is located the highly conserved phenylalanine, corresponding to Phe 393 of P450 BM3 (grey box). Two of the known P450s lacking this phenylalanine are also shown, where the phenylalanine is replaced by a tryptophan (*10*) or a proline (*11*) (solid box).

highlights the importance of this residue, yet, to date, no satisfactory explanation as to its role has been made. Previously, the aromatic side chain of the corresponding phenylalanine in P450 cam (F350) was proposed to participate directly in electron transfer to the P450 heme in a cytochrome b_5/P450 complex (*12*). Mutagenesis of this phenylalanine in rat liver P450 1A2 (F449) and rabbit P450 2E1 (F429) and subsequent characterization of the mutant enzymes led the investigators to different conclusions (with respect to P450 cam) regarding its role. In P450 1A2, F449 mutants showed diminished catalytic capacity and were affected in heme binding (*13*). In P450 2E1, only an effect on heme binding was observed in F429 mutants (*14*). However, neither study has conclusively resolved the question as to the conserved phenylalanine's importance in the catalytic competence of P450s. To elucidate its role, we describe here a series of comprehensive studies, characterizing both the kinetic and thermodynamic properties of site-directed mutants at phenylalanine 393 in flavocytochrome P450. Our results indicate that F393 is not essential for heme incorporation, but does have a key role in controlling the electronic properties of the heme system. We postulate that the interaction between this residue and the heme iron−sulfur bonding system is central to the control of the reactivity of oxygen with the ferrous heme.

EXPERIMENTAL PROCEDURES

Escherichia coli Strains and Plasmid Vectors. Escherichia coli TG1 [*sup*E, *hsd*Δ5, *thi*, Δ(*lac-pro*AB), F′ [*tra*Δ36, *pro*AB$^+$, *lac*I^q, *lac*ZΔM15]] was used for all cloning work and for overexpression of intact P450 BM3 and its component cytochrome domain. The preparation of plasmids for the overexpression of intact P450 BM3 (pBM23) and heme domain (P450, residues 1−472; pBM20) has been described in previous publications (*15*, *16*). Mutants F393A, F393H, and F393Y (intact) and F393A-HD, F393H-HD, and F393Y-HD (HD denotes heme domain) were constructed by oligonucleotide-directed mutagenesis of pBM23 and pBM20 respectively, using the Kunkel method (*17*, *18*). Single-stranded DNA was prepared using the helper phage M13KO7. Oligonucleotide primers used in the mutagenesis procedures were as follows (mismatches are indicated by the underlined bases and the names of the resulting expression plasmids are in parentheses): F393A and F393A-HD (pCM36, pCM80), 5′CTGACCGTTTCCAGCCGGTTTAAACGC 3′; F393H and F393H-HD (pCM 37, pCM81), 5′ CTGACCGTTTCCATGCGGTTTAAACGC 3′; F393Y,and F393Y-HD (pCM 109, pCM125), 5′ CCGTTTCCATACGGTTTAAAC 3′.

To ensure that no secondary mutations had occurred, pCM 36, pCM37, and pCM109 were sequenced by the dideoxy chain termination method. These plasmids were digested with restriction enzymes *Sna*BI and *Spe*I, generating a 3 kbp fragment containing the required mutation. The *Sna*BI/*Spe*I fragment was then ligated with the 4 kbp band liberated from a similar digestion of pBM23 (containing the WT P450 BM3 coding sequence under the control of the native CYP102 promoter) generating pJM1, pJM2, and pJM3, respectively.

Mutants were overexpressed in *E. coli* strain TG1 in an identical fashion to the wild-type clone.

Enzyme Preparations. All flavocytochromes P450 (wild-type and mutants) were purified from *E. coli* TG1 transformants (which express the P450 to high levels in the stationary phase under the control of the authentic promoter from *Bacillus*) by growth of transformant cultures (2−5 L of Luria-Bertani medium at 37 °C with shaking at 200 rpm) for ∼36 h after entry into the stationary phase. For the heme domains of wild-type and mutants, cells were induced (1 mM IPTG) at an $A_{600} = 1$, and growth was continued for 6−12 h prior to harvesting cells. Cells were disrupted by sonication. A similar purification protocol was employed for all enzymes using ion-exchange chromatography on DEAE-Sephacel and hydroxyapatite, as described previously (*19*). A final step (HiLoad 26/10 Q-Sepharose high performance column attached to a Pharmacia FPLC system, with protein elution gradient 0 to 500 mM KCl in 50 mM Tris·HCl/1 mM EDTA, pH 7.4) was employed to maximize the final purity of all the proteins. PMSF (1 mM) was added to all buffers to minimize proteolysis. All pure proteins were concentrated to >500 μM by ultrafiltration and were stored at −20 °C after dialysis against two successive 500-fold volumes of buffer A (50 mM Tris HCl, pH 7.4) containing 50% (v/v) glycerol. Enzymes were used within 1 month of isolation.

Spectrophotometric Analysis of Fatty Acid and Carbon Monoxide Binding to P450s. UV−vis absorption spectra were recorded over the 300−800 nm range using a Shimadzu 2101 spectrophotometer and quartz cuvettes of 1 cm path length. Typically, the concentration of wild-type or mutant P450 BM3 used was 1−5 μM in 1 mL of assay buffer (20 mM MOPS/100 mM KCl pH 7.4) at 30 °C.

Fatty Acid Binding Titrations. For enzyme titrations with arachidonic acid, aliquots (0.1−0.5 μL; not exceeding 3 μL total addition) of a 33 mM solution (in ethanol) were added to the enzyme solution (1−5 μM in assay buffer). For enzyme titrations with sodium laurate, 10 μL aliquots of P450 BM3 (1−5 μM in assay buffer) were withdrawn and replaced with aliquots of a solution of enzyme at identical concentration in the same buffer, but containing in addition 1 mM

sodium laurate. Spectra were recorded after each addition of substrate. Difference spectra were generated by subtraction of each spectrum recorded from the substrate-free spectrum. Dissociation constant (K_d) values were determined by plotting the maximal absorbance changes calculated from each difference spectrum against the concentration of substrate, and fitting the data to a rectangular hyperbola using Origin software (Microcal).

Carbon Monoxide Binding. Fe−CO complexes of wild-type and the mutant enzymes were prepared in the same fashion. Proteins were reduced by the addition of a few grains of sodium dithionite and were converted to the P450-complex by slow bubbling of the solutions with carbon monoxide gas for one minute.

Steady-State Kinetics. All steady-state kinetic measurements were performed at 30 °C in assay buffer using 1 cm path-length quartz cuvettes. Initial rates of fatty acid (arachidonate and laurate) oxidation were measured as described previously (*20*), by monitoring the oxidation of NADPH at 340 nm (ϵ_{340} 6.21 mM^{-1} cm^{-1}) with 10−100 nM enzyme and NADPH at saturating concentration (200 μM). The initial arachidonate concentration was varied by addition of small volumes (<2.0 μL) from a 33 or 3.3 mM ethanolic stock using a 10 μL Hamilton gastight syringe (Hamilton, Reno, NV), and the initial laurate concentration was varied by dilution of a 1 mM aqueous stock. Rate measurements were converted into activity units, s^{-1} (mol of NADPH oxidized/s per mol of P450) and plotted against fatty acid concentration. Data were fitted to the Michaelis−Menten equation using Origin software.

Determination of Enzymatic Coupling Efficiency. The coupling efficiencies of wild-type and the F393A, F393H, and F393Y mutant holoenzymes were determined by negative-ion electrospray mass spectrometry. Turnover assays were performed on each P450 under limiting concentrations of NADPH and excess arachidonate and oxygen (980 μL of 20 mM MOPS, pH 7.4, 4 μL of 33 mM arachidonate, 5 μL of 19.7 mM NADPH, and 10 μL of 4 μM P450). Reactions were initiated by addition of P450. The air-saturated concentration of oxygen in aqueous solution was ∼260 μM (*21*). Under these conditions, NADPH consumption can only be coupled to product formation or oxygen reduction (due to the absence of other electron acceptors in the assay and with both [substrate] and [oxygen] in excess of [NADPH]). Samples of each reaction mixture were injected into the mass spectrometer (Micromass Platform electrospray mass spectrometer) and analyzed under the following conditions: ESI-ve, cone voltage = 35 V, acquired range 150−500 Da. The concentration of unreacted substrate (*m*/*z* 303) and hydroxylated substrate (*m*/*z* 319) in each reaction mixture was evaluated from the total ion current for each peak (MassLynx software). The concentration of NADPH was calculated from its absorption spectrum (ϵ_{340} = 6.21 mM^{-1} cm^{-1}). All appropriate controls were run, and under these conditions, no interfering signals from NADPH, buffer, or enzyme were observed, with monohydroxylated arachidonate being the only observable product. The reactions were performed at 30 °C and conditions were optimized so that each reaction proceeded to completeness (total consumption of NADPH) within 30 s of initiation by addition of the catalytic concentration of enzyme. The quoted percent coupling was calculated from the relative stoichiometries of NADPH consumed to product formed, and is an average of four separate experiments for each P450.

Pre-Steady-State Kinetics of Heme Reduction. Measurement of the rate of the first flavin-to-heme electron transfer step was performed at 30 °C as described previously (*16*) using CO-saturated buffers and monitoring the formation of the ferrous-CO adduct at 450 nm using an Applied Photophysics stopped-flow spectrophotometer (SX. 17MV). One syringe contained NADPH (200 μM) and the second syringe contained intact wild-type or mutant P450 BM3 (1−5 μM). Both syringes contained assay buffer of identical substrate concentration (arachidonate or laurate), previously deoxygenated (by bubbling extensively with oxygen-free nitrogen) and saturated with CO by bubbling for 5 min. Rates for each substrate concentration were obtained by fitting the progress curves obtained to a double exponential function using the Applied Photophysics. The k_{lim} values were calculated by plotting the observed rates (k_{obs}) at a variety of substrate concentrations against fatty acid concentration, and fitting the data to the Michaelis−Menten equation using Origin software.

Generation of the Oxy-Ferrous Complex. All experiments were conducted within a Belle Technology glovebox under a nitrogen atmosphere ([O_2] < 5 ppm). Samples of wild-type HD, F393A-HD, F393H-HD, and F393Y-HD (∼2 μM) were prereduced by addition of a few grains of sodium dithionite. Excess dithionite was removed by elution of the protein through an anaerobic Biorad Econo-pac 10DG gel-filtration column, pre-equilibrated with degassed 100 mM MOPS, pH 7.0, ensuring no direct reduction of oxygen by dithionite. Generation of the oxy-ferrous complex was attempted by addition of 2.6 μM O_2 (addition of a 10 μL aliquot of air-saturated buffer) to 1 mL of reduced P450 (2 μM). The reaction was monitored at 424 nm over a 300 s time period, using a Shimadzu Multispec 1501 diode array UV−vis spectrophotometer. Experiments were conducted at 15 °C.

Potentiometric Titrations. All redox titrations were conducted within a Belle Technology glovebox under a nitrogen atmosphere, with the oxygen concentration maintained at less than 5 ppm. Degassed, concentrated enzyme samples (WT-HD, F393A-HD, F393H-HD, and F393Y-HD) were eluted through an anaerobic Bio-Rad Econo-pac 10DG gel filtration column, preequilibrated with 100 mL of degassed buffer (100 mM potassium phosphate, pH 7.0) immediately upon admission of the sample to the glovebox. This ensured removal of all traces of oxygen. Enzyme solutions (∼20 μM in 10 mL total volume) were titrated electrochemically according to the method of Dutton (*22*) using sodium dithionite (from a 34 mM stock) as reductant and potassium ferricyanide (from a 18 mM stock) as oxidant. Mediators were added to facilitate electrical communication between enzyme and electrode, prior to titration. Typically, 7.0 μM 2-hydroxy-1,4-naphthoquinone, 0.3 μM methyl viologen, and 1.0 μM benzyl viologen were included in the 10 mL sample volume (to mediate in the range −95 to −195 mV, −380 to −480 mV, and −260 to −360 mV, respectively). After a sufficient equilibration period (typically 10−15 min) following each reductive/oxidative addition, visible spectra were recorded over a 300−800 nm range using a Shimadzu 2101 UV−vis spectrophotometer contained within the anaerobic environment. The electrochemical potentials of the equilibrated

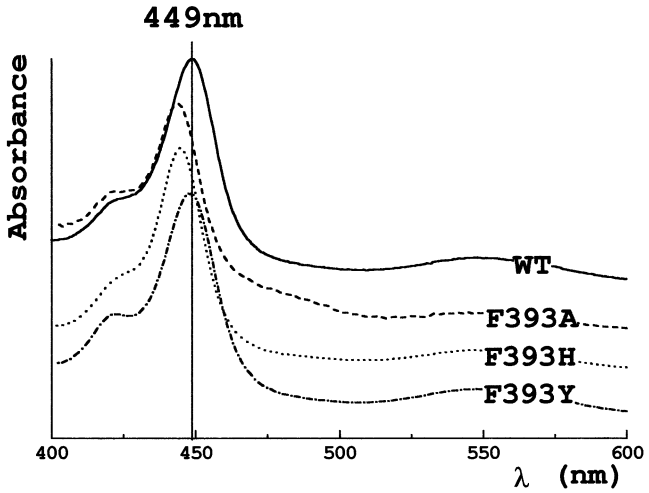

FIGURE 2: UV−vis spectra of the ferrous−CO complexes of wild-type P450 BM3 and F393A, F393H, and F393Y mutant forms. The spectra highlight the deviation in the position of the Soret absorption maximum. The spectra have been offset along the absorbance axis in the order indicated, for clarity. The Soret peak positions were blue-shifted by 4 nm (F393H), 5 nm (F393A), and 0 nm (F393Y) relative to that of wild-type (A_{max} = 449 nm, vertical line).

sample solutions were monitored using a CD740 meter (WPA) coupled to a Pt/calomel combination electrode (Russell pH Ltd.) at 25 ± 2 °C. The electrode was calibrated using the Fe^{3+}/Fe^{2+} EDTA couple as a standard (+108 mV). A factor of +242 mV was employed to correct relative to the standard hydrogen electrode. For substrate-bound redox titrations, arachidonate was added to the sample prior to the titration. Conversion to the high-spin form was observed spectrophotometrically as a shift from 418 to 390 nm. The K_M values for arachidonate for all the enzymes studied were much lower than 10 μM. Therefore, 33 μM arachidonate was sufficient in all cases to saturate the P450 (no further spin-state shift was observed upon further additions of substrate).

RESULTS

Overexpression and Purification of Mutant Enzymes. The successful overexpression and subsequent purification of the holoenzymes F393A, F393H, and F393Y, along with the heme domains (HD) F393A-HD and F393H-HD, immediately negated the previous assumption that phenylalanine 393 (Phe393) was essential for heme incorporation and stability. All mutant enzymes expressed to high levels, similar to wild-type, and remained stable when stored at −20 °C. All of the enzymes generated a native-like P450 absorbance spectrum, with no P420 contribution. An absorption peak at 420 nm would indicate the presence of enzyme with non-cysteine heme ligation.

Spectrophotometric Analysis of Carbon Monoxide Binding. Typically, treatment of a sample of reduced P450 with carbon monoxide will generate the characteristic P450−CO Soret absorption at 450 nm. This was the case for both wild-type P450 BM3 (A_{max} = 449 nm) and the most conservative mutant F393Y. However, a ~5 nm blue-shift in the P450−CO Soret absorption for mutants F393A (A_{max} = 444 nm) and F393H (A_{max} = 445 nm) was observed (Figure 2). This indicates a change in the strength, and hence the vibrational energy, of the CO bond, induced by changes in the degree of back-bonding from the ferrous heme iron to the CO antibonding orbitals. This is indicative of changes in the electron density at the iron. High electron density increases the degree of back-bonding to the CO antibonding orbitals, effectively weakening the CO bond, accompanied by a decrease in the Fe^{II}−CO vibrational energy (absorption would be red-shifted). A blue shift in the Fe^{II}−CO absorption is indicative of an increase in the strength of the CO bond (less back-bonding) as a direct result of a decrease in the electron density at the heme iron. Substitution of phenylalanine by either histidine or alanine appears to decrease the electron density of the heme iron, providing evidence that stabilization of the ferrous forms of mutants F393A and F393H is favored more so than in wild-type. The nature of the residue at position 393 appears to have an influence over this fundamental property of the heme. The most conservative substitution of phenylalanine (by tyrosine) does not appear to affect significantly the heme environment as its spectral properties are identical to wild-type.

Table 1: Substrate Dissociation Constants (K_d) for Wild-Type and F393 Mutants of P450 BM3[a]

	K_d (μM)			
	wild-type	F393A	F393H	F393Y
arachidonate	3.6 ± 0.3	2.6 ± 0.3	7.6 ± 0.5	4.2 ± 0.3
laurate	241 ± 9	230 ± 11	525 ± 10	520 ± 9

[a] Parameters were determined as described in the Experimental Procedures.

Fatty Acid Binding. The values for the dissociation constants for arachidonate and laurate binding to wild-type P450 BM3 and the mutant enzymes F393A, F393H, and F393Y are shown in Table 1. The major observation is that changing the nature of the side chain of residue 393 does not significantly alter the fatty acid-binding properties of the enzyme. This is intuitive considering the fact that the mutation is on the opposite side of the heme to the substrate-binding channel. Although mutations of Phe393 appeared to have little effect on substrate binding, differences in the degree of spin state shift (low- to high-spin) associated with the dehydration of the ferric iron center are apparent. For wild-type P450 BM3, there is a correlation between the degree of spin-state conversion and both the K_d and chain length of saturated fatty acid substrates. Fatty acids of chain length C_{15} and C_{16} (pentadecanoic and palmitic acids) have the lowest K_d values, and induce the largest degree of spin-state change. However, these substrates are highly insoluble in water. Lauric acid has better solubility in aqueous media (to approximately 1.2 mM) and has a K_d of ~250 μM. A much better substrate for P450 BM3 than any of the saturated fatty acids is the C_{20}, tetra-unsaturated arachidonic acid ($K_d \approx 4$ μM), which also has acceptable water solubility. Arachidonate induces a much greater spin-state shift than laurate (>95 and <40%, respectively). Comparisons between the mutants and wild-type P450 BM3 show differences in the degree of spin-state conversion with lauric acid. The arachidonate-induced (33 μM) spin-state shift for wild-type and all mutants was >95%, whereas the laurate-induced (1.0 mM) spin-state shift varies across the series F393A > F393Y > WT > F393H, with F393A giving ~12% higher proportion of the high-spin form than wild-type P450 BM3 (Figure 3).

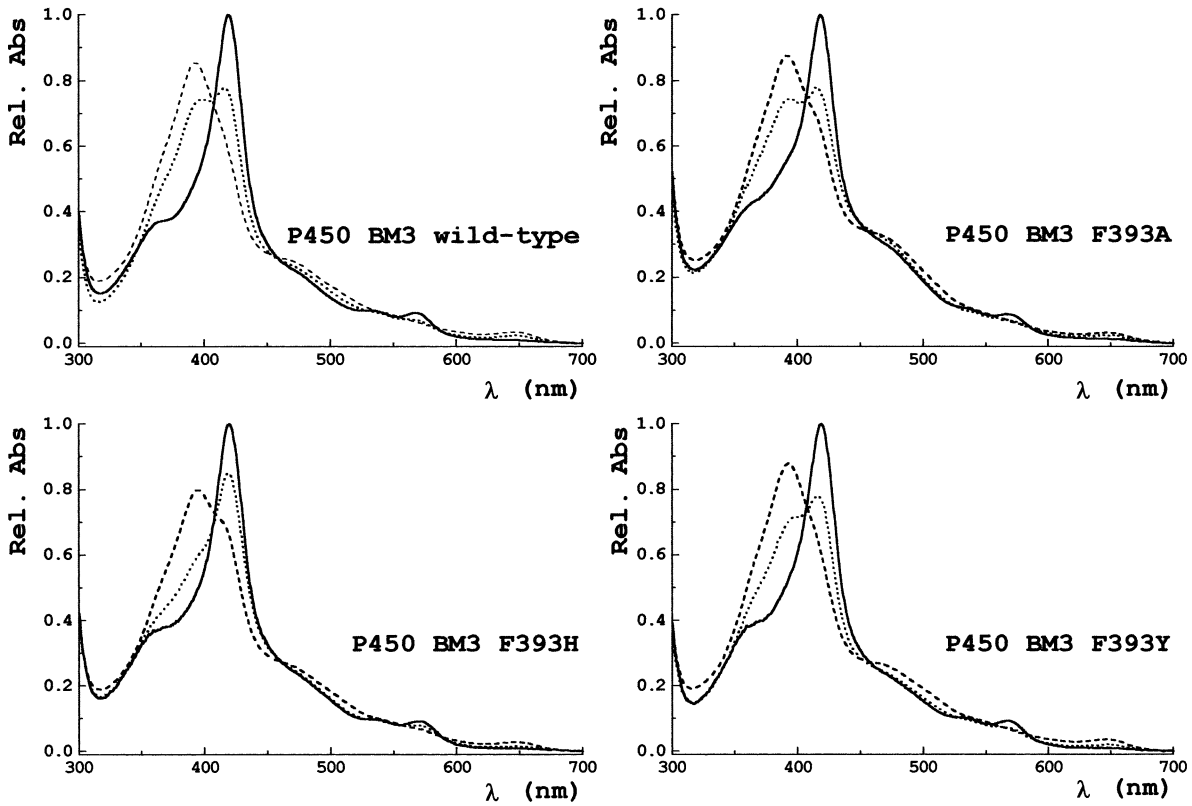

FIGURE 3: UV−vis spectra of the ferric (solid line), laurate (dotted line)-, and arachidonate-saturated (dashed line) forms of wild-type P450 BM3 and the F393A, F393H, and F393Y mutants. Rel. Abs. = relative absorbance compared to ferric Soret absorption maximum in each case. Arachidonate (33 μM) induces near-complete shift in spin-state in all forms. Laurate induces a much lower degree of spin-state shift in all enzymes, with F393H showing the smallest proportion of high-spin ferric heme at saturation with laurate (1 mM).

Table 2: Steady-State Kinetics of Fatty Acid (arachidonate and laurate)-Stimulated NADPH Oxidation by Wild-Type and F393 Mutant Flavocytochrome P450 BM3[a]

	wild-type		F393A		F393H		F393Y	
	K_M (μM)	k_{cat} (s^{-1})	K_M (μM)	k_{cat} (s^{-1})	K_M (μM)	k_{cat} (s^{-1})	K_M (μM)	k_{cat} (s^{-1})
arachidonate	4.7 ± 0.3	285 ± 3	2.7 ± 0.3	21 ± 1	3.8 ± 0.5	33 ± 1	9.5 ± 1.1	143 ± 8
laurate	288 ± 15	86 ± 2	18.5 ± 2.7	29 ± 1	60 ± 5	37 ± 1	274 ± 20	65 ± 2

[a] Parameters were determined as described in the Experimental Procedures.

Kinetics of Fatty Acid Oxidation. Although binding of the fatty acids was essentially unaffected by the nature of the residue at position 393, steady-state kinetic analysis shows significant differences in the rates of turnover of the mutant flavocytochromes compared to wild-type (Table 2). For both arachidonate and laurate oxidation, the observed trend in k_{cat} was WT > F393Y ≫ F393H > F393A. The differences in turnover are most obvious when arachidonate is the substrate, with 14-, 8-, and 2-fold decreases in k_{cat} for F393A, F393H, and F393Y, respectively, compared to wild-type P450 BM3. Although the magnitude of the difference between wild-type P450 BM3 and the mutants is smaller when laurate is the substrate, the trend is the same. Clearly some step in the catalytic cycle, other than substrate binding, has been perturbed and has become rate-limiting in the mutant enzymes.

The coupling efficiencies for wild-type, F393Y, and F393H (~90%) for arachidonate hydroxylation are all within experimental error of each other (Table 3) and suggest near exclusive coupling of NADPH oxidation to product formation. While the coupling of the F393A mutant is lower than the other P450s studied, this decrease cannot fully account for the order of magnitude difference observed between the steady-state parameters for the F393A mutant with respect to wild-type.

Table 3: Coupling Efficiency of the Wild-Type and F393 Mutant Holoenzymes in the Presence of Arachidonate, as Determined by Electrospray Mass Spectrometry[a]

	[unreacted substrate] (mM)	[product] (mM)	% coupling
wild-type	43 ± 3	89 ± 7	91 ± 11
F393A	77 ± 6	55 ± 5	56 ± 8
F393H	53 ± 4	79 ± 6	81 ± 10
F393Y	39 ± 3	93 ± 7	95 ± 11

[a] The concentrations of unreacted substrate and product were calculated from the total ion count for the negative ion of each relevent species in the mass spectrum, as outlined in the Experimental Procedures. In each case, the starting concentrations of arachidonate and NADPH were 132 and 99 μM, respectively. Percent coupling was determined from the relative stoichiometries of NADPH consumed to product generated.

This indicates that all enzymes are catalytically functional, and that the lowered catalytic activity observed for all the F393 mutants is due to decreased rate(s) of steps in the

Table 4: Pre-Steady-State Kinetics of Heme Reduction in Wild-Type and F393 Mutant Flavocytochromes P450 BM3[a]

	wild-type		F393A		F393H		F393Y	
	K_d (μM)	k_{lim} (s^{-1})	K_d (μM)	k_{lim} (s^{-1})	K_d (μM)	k_{lim} (s^{-1})	K_d (μM)	k_{lim} (s^{-1})
arachidonate	13.8 ± 2.0	348 ± 17	19.3 ± 3.5	1176 ± 78	13.3 ± 2.9	832 ± 53	6.4 ± 0.8	366 ± 11
laurate	300 ± 65	172 ± 14	124 ± 13	468 ± 11	291 ± 37	439 ± 20	400 ± 42	215 ± 10

[a] Rates were determined in the presence of both arachidonate and laurate substrates as described in the Experimental Procedures.

catalytic cycle after substrate binding and not as a result of the uncoupled reduction of oxygen.

Kinetics of Heme Reduction. To investigate whether the kinetics of flavin-to-heme electron transfer in the F393 mutants was affected, we undertook stopped-flow experiments to determine the rate of this process. The rate of the first electron-transfer step from the reductase FMN to the substrate-bound P450 BM3 heme can be conveniently measured using CO-saturated buffer, monitoring the formation of the ferrous iron-CO adduct at 450 nm (16). For each of the mutant flavocytochromes (F393A, F393H, and F393Y), the rate of flavin-to-heme electron transfer at 30 °C was measured by rapid mixing of CO-saturated solutions of (a) NADPH (200 μM) and substrate (either arachidonate at concentrations between 0 and 80 μM, or laurate at concentrations between 0 and 1000 μM) and (b) wild-type or mutant flavocytochrome (1−5 μM) and substrate (equal concentration to mixture a). The observed initial fast-phase rate constants (k_{obs}) for heme reduction were plotted against substrate concentration and fitted to a rectangular hyperbola. From these data, maximal apparent rates of first electron transfer to the heme iron (k_{lim}) and apparent dissociation constants for the substrates (K_d) were obtained and are shown in Table 4. The trend in k_{lim} F393A > F393H ≫ F393Y ≈ WT was the reverse of that observed for the steady-state turnover of both laurate and arachidonate. Thus, although steady-state experiments suggest an overall decrease in the turnover rates of these F393 mutant enzymes, the first flavin-to-heme electron transfer reaction is actually faster in all the mutant enzymes than in wild-type. In the wild-type P450 BM3, the apparent rate of flavin-to-heme electron transfer (as measured by the formation rate of the ferrous-CO adduct) is 348 s^{-1}, where the overall turnover rate of the enzyme is 285 s^{-1} (in the presence of arachidonate). Clearly, this microscopic rate is the major determinant of catalytic turnover rate, as observed previously (*19*). However, with the F393A and F393H mutants, the situation is markedly different. For instance, in F393A, the flavin-to-heme rate is 1176 s^{-1} but the steady-state rate is only 21 s^{-1}. Evidently, a step after the first electron transfer to the heme iron has become rate limiting in these mutants.

Generation of the Oxy-Ferrous Complex of F393A-HD. Binding of oxygen to the ferrous wild-type heme domain and F393Y-HD was too transient to be monitored on a macroscopic time scale. Addition of oxygenated buffer to the prereduced protein led to immediate oxidation to the ferric resting state, without noticeable formation of any oxy-ferrous intermediate. This was unsurprising considering that the oxy-ferrous intermediate has only been transiently observed for wild-type P450 BM3 at cryogenic temperatures (*23*). However, the formation of the oxy-ferrous complex for the F393A-HD and F393H-HD was observed (Figure 4) and had a half-life of approximately 30 s. This result provides evidence that the reaction between oxygen and the ferrous iron is significantly faster in wild-type and F393Y than in either F393A or F393H. It also suggests an increase in the stability of the ferrous-form of the F393A and F393H mutants with respect to wild-type, allowing the stable binding of oxygen to the heme for a appreciable period prior to eventual reoxidation of the heme. This supports the idea that the substitution of phenylalanine 393 alters considerably the reactivity of the P450 heme with molecular oxygen.

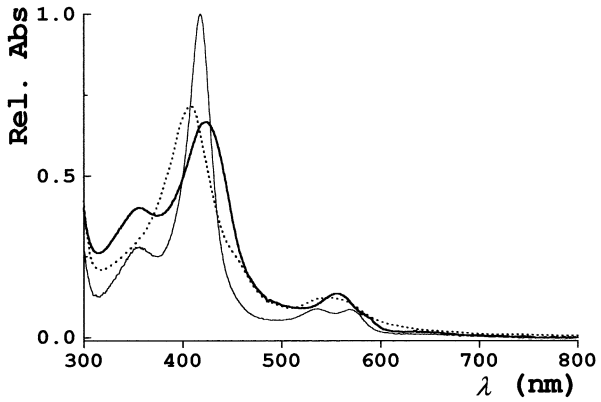

FIGURE 4: UV−vis spectra showing formation of the stable oxy-ferrous intermediate of P450 BM3 F393A mutant. The spectra were generated prior to (ferrous, dotted line), immediately after (oxy-ferrous, heavy solid line), and 300 s after (low-spin ferric, light solid line) addition of 2.6 μM oxygenated buffer to a sample of prereduced protein.

Heme Domain Potentiometric Titrations. The substrate-free and arachidonate-saturated (33 μM) reduction potentials of wild-type HD, F393A-HD, F393H-HD, and F393Y-HD were measured in an attempt to establish effects of the mutations on the thermodynamic properties of these variants. Figure 5 shows the spectral shifts observed during the course of these potentiometric titrations. At the high P450 concentration (~20 μM) required for efficient communication between the P450/mediators/electrode, the absorption at the Soret maximum is much too high for accurate spectrophotometric measurement. A convenient part of the spectrum that reflects accurately the change in reduction state of the heme iron at this P450 concentration is the region between 460 and 470 nm. Therefore, data for the substrate-free titrations at 465 nm were plotted against measured potential (mV vs SHE). Due to the spectral differences generated upon addition of substrate to the enzymes, substrate-saturated titrations were evaluated differently, plotting the difference in absorbance $A_{484} - A_{730}$ against measured potential (Figure 6). Data were fitted to a one-electron Nernst function, and values obtained are presented in Table 5. The first observation is that the reduction potential of the wild-type P450 BM3 heme iron has been more accurately re-determined in light of improved experimental techniques. The more negative reduction potential determined fits better to the proposed redox organization within P450 BM3. At this potential, the substrate-induced redox switch (*24*) can still operate, since

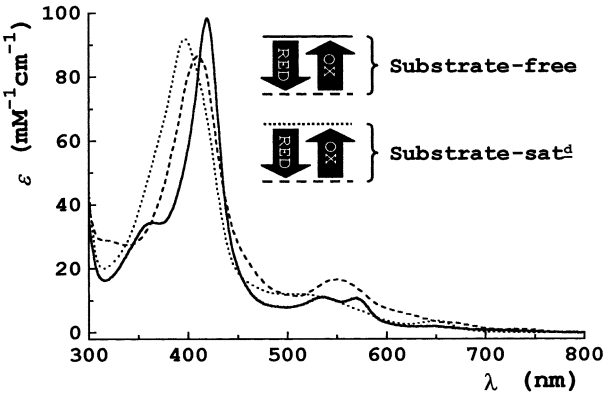

FIGURE 5: UV−vis spectra showing spectral changes associated with reduction of substrate-free (low-spin) and substrate (arachidonate)-saturated P450 BM3 (high-spin) heme domain. For the wild-type ferric enzyme (solid line), the substrate-free Soret maximum is at 418 nm, and for the substrate-bound form (dotted line) it is located at 390 nm. In both cases, the fully reduced ferrous form (dashed line) has its Soret maximum at approximately 410 nm. The millimolar extinction coefficients of the different species are indicated. The reduction of all heme domains was freely reversible (reduction by dithionite, oxidation by ferricyanide) with minimal hysteresis. Complete reoxidation of the ferrous-form results in the regeneration of the initial starting spectra (ferric low- or high-spin).

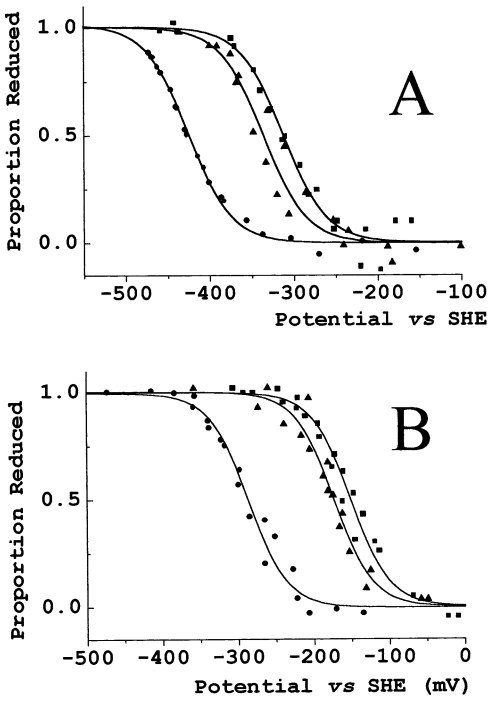

FIGURE 6: Heme-domain reduction potentials of wild-type and mutant P450s BM3. Overlaid, normalized one-electron Nernst curves showing the changes in the proportion of reduced species with reduction potential (vs standard hydrogen electrode) are presented. The data for F393Y-HD is essentially identical to WT-HD, and has been omitted for clarity. From these, the midpoint potentials of the substrate-free (A) and arachidonate-saturated (B) wild-type heme domain (circles), F393A-HD (squares), and F393H-HD (triangles) were determined (Table 5). The measured heme reduction potentials of both the F393A-HD and F393H-HD (substrate-free and substrate-saturated) mutants are considerably more positive than wild-type heme domain (between 95 and 138 mV) suggesting stabilization of their ferrous forms. The substrate-induced redox shift, observed for wild-type (*24*), still operates in the F393A, F393H mutants (whereby addition of substrate causes a 138−161 mV increase in the reduction potential), suggesting that substrate binding exerts the same type of control over the heme reduction potential as observed in wild-type. The nature of the residue at position 393 appears to control the thermodynamic properties of the heme.

binding of substrate increases the reduction potential by 138 mV (to −289 mV) allowing electron transfer from NADPH, through the reductase and ultimately to the heme. However, there is tighter control than previously imagined over uncoupling by virtue of the fact that the substrate-free heme potential is considerably more negative than that of the physiological electron donor NADPH (−320 mV) in the low-spin ferric form of wild-type P450 BM3. The midpoint potentials of the two mutants F393A and F393H are considerably more positive than wild-type (−312 and −332 mV, respectively) and both display similar magnitudes of reduction potential shift upon substrate binding to wild-type (∼140−160 mV shift). The more positive heme reduction potentials of these two mutants are also consistent with the higher rates of flavin-to-heme electron transfer observed. A thermodynamic consequence of the more positive reduction potentials of the heme iron is an increase in the stabilization of the ferrous form. This is borne out by the ability to generate the ferrous form (A_{max} = 410 nm) for the F393H and F393A mutant P450s aerobically, whereas this is achievable only under strictly anaerobic conditions for the wild-type P450 BM3. It is notable that the increase in reduction potential correlates to the relative size of the side chain at position 393. As the steric bulk is decreased (Phe/Tyr → His → Ala), the reduction potential increases accordingly (−427/-418 → −332→ −312 mV).

Table 5: Midpoint Heme Reduction Potentials for Substrate-Free and Arachidonate-Saturated Wild-Type and F393 Mutant P450s BM3

	midpoint potential (mV)			
	WT-HD[a]	F393A-HD	F393H-HD	F393Y-HD
substrate-free	−427 ± 4	−312 ± 4	−332 ± 6	−418 ± 6
arachidonate-sat[d]	−289 ± 5	−151 ± 4	−176 ± 4	−295 ± 6

[a] HD denotes heme domain.

DISCUSSION

Phenylalanine 393 of P450 BM3 is one of only a small number of residues highly conserved throughout the P450 superfamily. While previous mutagenesis studies have been performed to characterize mutants at this position in other P450s (e.g., 2E1, 1A2) (*13*, *14*) no satisfactory explanation has been offered as to why this residue should be a phenylalanine or how this residue may influence P450 mechanism. What is clear (in the case of P450 BM3 as well as those P450s studied previously) is that changing the nature of this residue has severe implications on the catalytic competence of the resultant mutants compared with native forms. The purpose of our study was to attempt to resolve the role of this conserved phenylalanine using the flavocytochrome P450 BM3 system. Certain parallels can be drawn between our data and those reported previously for mutants of P450 1A2 (e.g., similar blue-shifts in the ferrous-CO spectra) (*13*) and P450 2E1 (slower turnover kinetics) (*14*). However, in the light of our studies, it is clear that previous assumptions made as to the role of the phenylalanine (decreased enzyme stability and alteration of electron flow) are unlikely to fully account for the observed decreases in

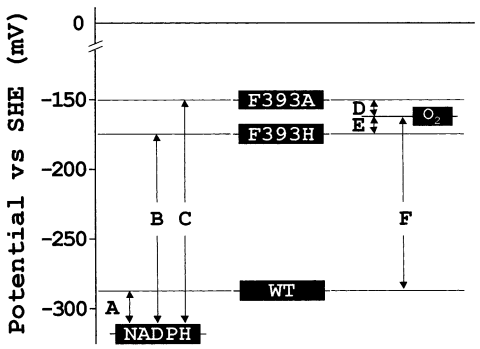

FIGURE 7: Diagrammatic representation of relevant reduction potentials in the P450 BM3 system. The reduction potentials of NADPH (−320 mV), the arachidonate-saturated heme domains of wild-type (−289 mV), F393A (−151 mV), F393H (−176 mV), and the one electron reduction potential of oxygen to superoxide (−160 mV) are presented. A much greater driving force is associated with heme reduction for the mutants F393A/H (B, C) compared to wild-type (A), while the gap in reduction potential associated with oxygen reduction is much smaller for the mutants F393A/H (D, E) compared to wild-type (F).

catalytic activity. It is clear that F393 plays a much more important and fundamental role—by controlling the ability of P450 BM3 to bind and activate molecular oxygen.

The successful overexpression of F393A, F393H, and F393Y mutants demonstrates the lack of a requirement for a phenyl ring to stabilize heme binding. Also, the kinetic profiles of these mutant enzymes dismisses the argument that this residue is essential in facilitating electron transfer to the heme. We have shown that while the F393A and F393H enzymes are less catalytically competent (lower turnover rate), the study of individual steps in the catalytic cycle reveals that the rate of heme reduction is actually faster for these mutants than for wild-type. Thus, replacement of the phenylalanine can actually elevate the rate of heme reduction. Hence, contrary to previous suggestions, the residue is nonessential for mediation of electron transfer, either directly or indirectly, to the heme. It is not required absolutely for electron transfer, but instead plays a vital role in the control of the process. The question is then one of how this control is achieved. The most convenient starting point for discussion is with the thermodynamic data obtained from the potentiometric titrations. All other results are consistent with, and can be explained in light of, data from these experiments.

Substitution of phenylalanine 393 by either histidine or alanine results in an increase of the heme iron reduction potential with respect to wild-type P450 BM3, whereas the reduction potential is unchanged upon substitution by tyrosine. This explains the apparent contradiction in effects on steady state (decreased) and heme reduction (increased) kinetic rates observed for the mutants relative to wild-type P450 BM3. Creating a large positive gap in reduction potential between the electron donor [NADPH at −320 mV ultimately providing the electron(s) to the FMN semiquinone at -213 ± 5 mV] and the substrate-bound heme (e.g., -151 ± 4 mV for F393A) increases the driving force (ΔG) for heme reduction in this system (Figure 7). The observed increase in pre-steady-state flavin-to-heme electron-transfer kinetics ($k_{lim} = 1180\ s^{-1}$ cf. $348\ s^{-1}$ for wild-type P450 BM3) is totally consistent with the more positive reduction potentials of heme iron (suggesting stabilization of the ferrous form) in the F393A and F393H mutants. However, the fact that F393A and F393H mutants give much lower steady-state rates of fatty acid-dependent NADPH oxidation is explained by the concomitant decrease in driving force for molecular oxygen to superoxide (−160 mV, Figure 7). Thus, whereas having alanine or histidine at position 393 facilitates faster electron transfer to the heme iron, the rate at which the ferrous iron can then reduce bound molecular oxygen is much lowered, with a net large decrease in enzyme turnover rate.

Substrate affinity for these mutant enzymes is not significantly perturbed compared to wild-type, and the rate of substrate-induced spin-state change is known to be rapid from previous studies (*16*). For wild-type P450 BM3, the rate of first electron transfer to the ferric heme ($348\ s^{-1}$ with arachidonate) is similar to the steady-state k_{cat} for turnover of this substrate ($285\ s^{-1}$), indicating that the sequence of events leading to the first electron transfer to the heme plays a major role in turnover rate limitation. In contrast, in the F393A and F393H mutants, not only are the rates of heme reduction elevated (1176 and $832\ s^{-1}$, respectively, with arachidonate), but the steady-state turnover rates are diminished (21 and $33\ s^{-1}$, respectively). Obviously, there is a new major factor in overall rate limitation that occurs after the first heme reduction and, presumably, does not involve substrate binding. This factor almost certainly reflects the increased stability of the oxy-ferrous form in the mutants. The elevated reduction potential of their hemes results in decreased driving force for reduction of bound dioxygen, leading to the oxy-ferrous form being considerably more stable than the superoxy-ferric form. This is borne out by the observation that in the mutants with the most positive heme reduction potential (F393A and F393H), the substrate-saturated, oxy-ferrous form is not only observable ($A_{max} =$ 424 nm), but also has a long half-life ($\sim$ 30 s) at 15 °C. Under similar conditions, the decay of the oxy-ferrous form of wild-type P450 BM3 is virtually instantaneous, and even at cryogenic temperatures, the species can be observed only transiently (*23*). The consequence of the elevated heme reduction potential in F393A and F393H is that oxygen activation is disfavored and that the stabilized oxy-ferrous intermediate becomes a thermodynamic trap, which decreases the rate of overall catalysis. It appears likely that, in these mutants, oxygen reduction replaces heme reduction as the overall rate-limiting step.

In conclusion, we have established for flavocytochrome P450 BM3 that the phylogenetically conserved phenylalanine residue F393 has an important role in control of the reduction potential of the P450 heme iron. As evidenced by a combination of steady-state and stopped-flow studies, we have shown that the ability to poise the heme potential appropriately is critical for efficient catalysis. The physical origin of these catalytic modifications is still unclear and are presently under investigation. In ongoing studies, we are characterizing site-directed mutant F393W. In the nitric oxide synthases (NOSs), a tryptophan residue is conserved in place of the phenylalanine (*25*). Analysis of this mutant may allow a clearer understanding of the differences in catalytic properties of NOS and the P450s.

ACKNOWLEDGMENT

The authors wish to thank Dr. S. N. Daff for his useful and constructive discussions.

REFERENCES

1. Munro, A. W., and Lindsay, J. G. (1996) *Mol. Microbiol. 20*, 1115−1125.
2. Unger, B. P., Gunsalus, I. C., and Sligar, S. G. (1986) *J. Biol. Chem. 261*, 1158−1163.
3. Narhi, L. O., and Fulco, A. J. (1986) *J. Biol. Chem. 261*, 7160−7169.
4. Poulos, T. L., Finzel, B. C., and Howard, A. J. (1986) *Biochemistry 25*, 5314−5322.
5. Ravichandran, K. G., Boddupalli, S. S., Hasemann, C. A., Peterson, J. A., and Deisenhofer, J. (1993) *Science 261*, 731−736.
6. Mueller, E. J., Loida, P. J., and Sligar, S. G. (1995) Twenty five years of P450 cam research. in *Cytochrome P450: Structure, Mechanism and Biochemistry* (Ortiz de Montellano, P. R., Ed.) pp 83−124, Plenum Press, New York.
7. Narhi, L. O., and Fulco, A. J. (1987) *J. Biol. Chem. 262*, 6683−6690.
8. Li, H. Y., Raman, C. S., Glaser, C. B., Blasko, E., Young, T. A., Parkinson, J. F., Whitlow, M.; Poulos, T. L. (1999) *J. Biol. Chem. 274*, 21276−21284.
9. Nelson, D. R., Koymans, L., Kamataki, T., Stegeman, J. J., Feyereisen, R., Waxman, D. J., Waterman, M. R., Gotoh, O., Coon, M. J., Estabrook, R. W., Gunsalus, I. C., and Nebert, D. W. (1996) *Pharmacogenetics 6*, 1−42.
10. Song, W.-C., Funk, C. D., and Brash, A. R. (1993) *Proc. Natl. Acad. Sci. U.S.A. 90*, 8519−8523.
11. Teunissen, Y., Geraerts, W. P. M., van Heerikhuizen, H., Planta, R. J., Joosse, J. (1992) *J. Biochem. 112*, 249−252.
12. Stayton, P. S., Poulos, T. L., and Sligar, S. G. (1989) *Biochemistry 28*, 8201−8205.
13. Shimizu, T., Hirano, K., Takahashi, M., Hatano, M., and Fujii-Kuriyama, Y. (1988) *Biochemistry 27*, 4138−4141.
14. Porter, T. D. (1994) *Biochemistry 33*, 5942−5946.
15. Miles, J. S., Munro, A. W., Rospendowski, B. N., Smith, W. E., McKnight, J., and Thomson, A. J. (1992) *Biochem. J. 288*, 503−509.
16. Munro, A. W., Daff, S., Coggins, J. R., Lindsay, J. G., and Chapman, S. K. (1996) *Eur. J. Biochem. 239*, 403−409.
17. Kunkel, T. A. (1985) *Proc. Natl. Acad. Sci. U.S.A. 82*, 488−492.
18. Zoller, M. J., and Smith, M. (1983) *Methods Enzymol. 100*, 468−500.
19. Noble, M. A., Miles, C. S., Chapman, S. K., Lysek, D. A., Mackay, A. C., Reid, G. A., Hanzlik, R. P., and Munro, A. W. (1999) *Biochem. J. 339*, 371−379.
20. Munro, A. W., Noble, M. A., Miles, C. S., Daff, S. N., Green, A. J., Quaroni, L., Rivers, S., Ost, T. W. B., Reid, G. A., and Chapman, S. K. (1999) *Biochem. Soc. Trans. 27*, 190−196.
21. Abu-Soud, H. M., Ichimori, K., Presta, A., and Stuehr, D. J. (2000) *J. Biol. Chem. 275*, 17349−17357.
22. Dutton, P. L. (1978) *Methods Enzymol. 54*, 411−435.
23. Bec, N., Anzenbacher, P., Anzenbacherova, E., Gorren, A. C. F., Munro, A. W., and Lange, R. (1999) *Biochem. Biophys. Res. Commun. 266*, 187−189.
24. Daff, S. N., Chapman, S. K., Turner, K. L., Holt, R. A., Govindaraj, S., Poulos, T. L., and Munro, A. W. (1997) *Biochemistry 36*, 13816−13823.
25. Adak, S., Crooks, C., Wang, Q., Crane, B. R., Tainer, J. A., Getzoff, E. D., and Stuehr, D. J. (1999) *J. Biol. Chem. 38*, 26907−26911.
26. Wen, L. P., and Fulco, A. J. (1987) *J. Biol. Chem. 262*, 6676−6682.
27. Feyereisen, R., Koener, J. F., Farnsworth, D. E., and Nebert, D. W. (1989) *Proc. Natl. Acad. Sci. U.S.A. 86*, 1465−1469.
28. Andersson, S., Davis, D. L., Dahlbäck, H., Jörnvall, H., and Russell, D. W. (1989) *J. Biol. Chem. 264*, 8222−8229.
29. Chung, B., Matteson, K. J., Voutilainen, R., Mohandas, T. K., and Miller, W. L. (1986) *Proc. Natl. Acad. Sci. U.S.A. 83*, 8962−8966.

BI010716M